

## Study of the Modified Gaussian Model on olivine diagnostic spectral features and its applications in space weathering experiments

Hui-Jie Han (韩慧杰)<sup>1</sup>, Xiao-Ping Lu (卢晓平)<sup>1</sup>, Ya-Zhou Yang (杨亚洲)<sup>2</sup>, Hao Zhang (张昊)<sup>3,4</sup> and Admire Muchimamui Mutelo<sup>5</sup>

<sup>1</sup> State Key Laboratory of Lunar and Planetary Sciences, Macau University of Science and Technology, Taipa 999078, Macau, China; [xplu@must.edu.mo](mailto:xplu@must.edu.mo)

<sup>2</sup> State Key Laboratory of Space Weather, National Space Science Center, Chinese Academy of Sciences, Beijing 100190, China

<sup>3</sup> Planetary Science Institute, School of Earth Sciences, China University of Geosciences, Wuhan 430074, China

<sup>4</sup> CAS Center for Excellence in Comparative Planetology, Hefei 230026, China

<sup>5</sup> School of Earth Science and Resources, China University of Geosciences, Beijing 100083, China

Received 2019 November 7; accepted 2020 March 15

**Abstract** The absorption features of olivine in visible and near-infrared (VNIR) reflectance spectra are the key spectral parameters in its mineralogical studies. Generally, these spectral parameters can be obtained by exploiting the Modified Gaussian Model (MGM) with a proper continuum removal. However, different continua may change the deconvolution results of these parameters. This paper investigates the diagnostic spectral features of olivine with diverse chemical compositions. Four different continuum removal methods with MGM for getting the deconvolution results are presented and the regression equations for predicting the Mg-number (Fo#) are introduced. The results show that different continua superimposed on the mineral absorption features will make the absorption center shift, as well as the obvious alterations in shape, width and strength of the absorption band. Additionally, it is also found that the logarithm of a second-order polynomial continuum can match the overall shape of the spectrum in logarithmic space, and the improved regression equations applied to estimate the chemical composition of olivine-dominated spectra also have a better performance. As an application example, the improved approach is applied to pulse laser irradiated olivine grains to simulate and study the space weathering effects on olivine diagnostic spectral features. The experiments confirm that space weathering can make the absorption band center shift toward longer wavelength. Therefore, the Fo# estimated from remote sensing spectra may be less than its actual chemical composition. These results may provide valuable information for revealing the difference between the spectra of olivine grains and olivine-dominated asteroids.

**Key words:** techniques: spectroscopic — instrumentation: spectrographs — methods: statistical — minor planets, asteroids: general

### 1 INTRODUCTION

Hyperspectral remote sensing data are widely used in identification of minerals and rocks (Adams 1974; Singer 1981; Cloutis & Bell III 2000; Burbine et al. 2002; Basilevsky et al. 2012; Roush et al. 2015), especially on studies of the surface materials of the Moon, Mars and asteroids (Pieters & Mustard 1988; Bishop et al. 1998; Ohtake et al. 2009; Wu et al. 2010; Lindsay et al. 2015). The visible and near-infrared (VNIR) reflectance spectra are sensitive to the mafic mineral compositions (Lucey

2004; Staid et al. 2011). As a major mafic mineral, olivine is an important material in understanding the geologic evolutionary process of terrestrial bodies. It is the foremost mineral to crystallize from magma and form the major component of planetary mantles. Olivine bears rich information on the magma ocean. Olivine materials in the deep crust and mantle can be exposed to the crust or surface by a magmatic explosion and giant impacts (Tonks & Melosh 1992; Wilson & Head 2017), and detected by a remote sensing instrument. Furthermore, it was found that high Fo# ( $100 \times \text{Mg}/(\text{Mg}+\text{Fe})$ ) olivine indicates

a primordial magma of mantle origin, while low Fo# olivine signifies a differentiated and evolved magma (Taylor 1978; Shearer & Papike 1999). The composition of olivine is an indicator to study the mantle materials and planetary evolutionary history.

### 1.1 Olivine Spectroscopy

A visible and near-infrared spectrometer (VNIS) is often considered an essential instrument for orbital remote sensing. Generally, the VNIR spectra of absorbing minerals contain absorption bands that are characteristic of their compositions and crystal structures (e.g., Mustard et al. 2005; Pieters et al. 2009). The crystalline structure of olivine contains two different six-coordinated sites: the centrosymmetric M1 site and non-centrosymmetric M2 site (Burns 1970). In the series from fayalite to forsterite,  $\text{Mg}^{2+}$  and  $\text{Fe}^{2+}$  ions are randomly distributed within the two sites, and the  $\text{Fe}^{2+}/\text{Mg}^{2+}$  ratio can provide information on the differentiation process of the olivine (Burns 1974; Dyar et al. 2009). The presence of  $\text{Fe}^{2+}$  in the central absorption site M2 and two bilateral absorption sites M1–1 & M1–2 of the olivine crystal field make three spin-allowed transitions and form three corresponding characteristic absorption features in the VNIR spectrum near 0.87, 1.05 and 1.25  $\mu\text{m}$  (Hunt 1977; Hunt & Ashley 1979). The combination of these absorption bands results in a broad integrated diagnostic feature near 1.0  $\mu\text{m}$  (Fig. 1), and its useful spectral behavior finally makes olivine chosen for this study.

Identification of mafic mineral olivine is done by composition analysis of laboratory mineral samples and via satellite remote sensing detection (e.g., Mustard et al. 2005). The scientific study of olivine content, crystal structure and spectral features will help us to uncover the formation and evolution of planets and moons (e.g., Lucey et al. 1998; Yamamoto et al. 2010; Miyazaki et al. 2013; Ody et al. 2013; Li et al. 2019). Remote sensing can acquire a large amount of spectral information. However, the spectral data are not directly exploited, since the spectral analysis requires much prior knowledge with many attempts in the correction for absorption bands of minerals to fit different models (Antonenko & Cloutis 2003).

### 1.2 The Modified Gaussian Model (MGM)

The Modified Gaussian Model (MGM), originally developed and described by Sunshine et al. (1990), is based on physical processes in electronic transition absorptions and a statistical method to investigate the probability distribution. It is an automated mathematical method for deconvolving the superposed absorption features in reflectance spectra. MGM is a widely utilized model for accurately decomposing the mineral absorption features into their

physically isolated absorption bands, and can estimate the single mineral modal abundances within 5%~10% for mafic minerals and rocks (Sunshine & Pieters 1993). It has been successfully applied to interpret and quantify the compositional and abundance information on minerals or mineral mixtures, which make up the observed surface (e.g., Sunshine & Pieters 1998; Mustard et al. 2005; Jin et al. 2013). Many studies have applied and adapted the method based on experience and detailed explanation of the parameters of the resulting absorption band processed by this model (e.g., Pinet et al. 2009; Tsuboi et al. 2010; Sugita et al. 2011).

It is worth noting that implementing the MGM to analyze spectra in the wavenumber domain (spatial frequency or energy) is numerically equivalent to Gaussian analysis in wavelength (Gallie et al. 2008). In addition, it is necessary to pay attention to the constraints between the relative band absorption strengths. Each Gaussian curve must conform to the electronic transition absorption laws, while getting the optimal numerical solution. The MGM code applied in this paper is the version 2.0 MATLAB code, which calculates the best-fit bands employing the stochastic non-linear inverse algorithm developed by Tarantola & Valette (1982). The code can be downloaded from Brown University<sup>1</sup>.

MGM is very useful for planetary remote sensing data interpretations. Continuum removal as an important issue in spectral interpretation has still not been analyzed in detail with the MGM. Indeed, the continuum is superimposed on the mineral absorption features, which can cause the absorption center to shift, as well as obvious alterations in shape, width and strength of the absorption band (Rodger et al. 2012; Zhang et al. 2016). However, it seems to be using markedly different continuum line styles in the MGM deconvolution in Sunshine & Pieters (1998) and others (e.g., Noble et al. 2006; Clénet et al. 2011; Li et al. 2019). Different continua will make a change in the band center. In addition, the MGM deconvolution relies on relative band strength values and band center positions. Therefore, continua with different slopes and types will lead to different results for MGM deconvolution. So, it is necessary to study the effects of different continuum removal methods on MGM.

### 1.3 MGM and Space Weathering

Space weathering is the surface process that can cause physical and chemical changes on the surface of airless bodies (Hapke 2001). This process, including micrometeorite impacts and solar wind implantations, can darken, redden and reduce the contrast of the VNIR spectra

<sup>1</sup> <http://www.planetary.brown.edu/mgm/>

of most silicate minerals, and make the spectra difficult to interpret (Pieters et al. 1993; Chapman 2004). Researches have pointed out that “nanophase iron particles,” abbreviated as  $\text{npFe}^0$ , disassociation from iron-bearing minerals, produced by irradiation, and vapor deposition effects, can cause changes in the optical properties and chemical composition on the material surface (Pieters et al. 2000; Hapke 2001; Brunetto et al. 2006; Fu et al. 2012; Yang et al. 2017).

At present, pulsed laser irradiation and ion bombardment are the common experimental simulation methods for space weathering simulation (e.g., Kohout et al. 2014). These have been used to simulate space weathering on olivine grains for interpreting the material composition of lunar soil, A-type asteroids and S-type asteroids (e.g., Chapman 1996; Pieters et al. 2000; Chapman 2004). MGM is widely applied to reveal the surface mineralogy of asteroids (e.g., De Leon et al. 2004; Sunshine et al. 2004, 2007; Binzel et al. 2009; Wang et al. 2017). However, space weathering will complicate the interpretations of telescopic spectra of asteroids (Clark et al. 2002; Chapman 2004). So far, only a handful of studies optimized the effects of space weathering on MGM deconvolution results. For example, Fu et al. (2012) studied the effects of space weathering on mineral diagnostic spectral features based on the results of  $\text{He}^+$  irradiation experiments and pointed out that the diagnostic band centers shift to longer wavelength after radiation. There is a need for more experiments based on application of the MGM approach in space weathering.

In this work, firstly we collected spectral data of olivine with different particle sizes and compositions, solid solutions ranging from fayalite ( $\text{Fe}_2\text{SiO}_4$ ) to forsterite ( $\text{Mg}_2\text{SiO}_4$ ), and then examined different continuum removal methods employed for MGM analysis. Secondly, we investigated the effects of space weathering on MGM analysis by examining the spectra of laser-irradiated olivine and olivine-dominated A-type asteroids (246) Asporina and (354) Eleonora.

## 2 DATA AND METHODS

### 2.1 VNIS Spectra and Composition of the Olivine Solid Solution

The spectral laboratory data described here are provided by the U.S. Geological Survey (USGS)<sup>2</sup> and RELAB Spectral Database is supported by NASA<sup>3</sup>. The USGS M3t data were processed with the spectral characteristics determined by Green et al. (2011), who convolved the mineral

<sup>2</sup> <https://speclab.cr.usgs.gov/spectral-lib.html>

<sup>3</sup> <http://www.planetary.brown.edu/relab/>

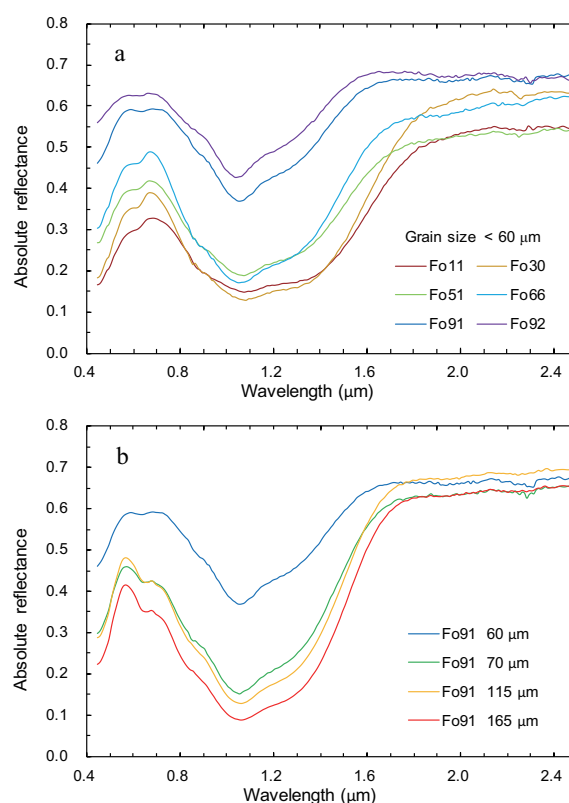


**Fig. 1** Reflectance spectra of olivine. Panel a: Olivine of varied Fo# with same grain size, all spectra are for  $<60\ \mu\text{m}$  size powders, showing increasing reflectance and decreasing band depth with increasing Fo#; Panel b: Olivine spectra of varied Fo# with varied grain size (60 to  $165\ \mu\text{m}$ ), exhibiting decreasing reflectance with increasing grain size.

spectral data with the target mode of the Moon Mineralogy Mapper ( $\text{M}^3$ ) spectrometer.

The spectra of olivine with several different size distributions are considered in this study. The olivine sample ID and information are listed in Table 1. Seven samples, with IDs like K1xxxx, were also used in Sunshine & Pieters (1998). One should note that Fo# was recalculated according to the chemical composition of the USGS olivine samples. The recalculated Fo# values are a little different from the stated sample values. For accuracy, the recalculated Fo# was applied in this study. Olivine spectra in the RELAB Spectral Database are synthetic samples, as described by Dyar et al. (2009), and the Fo# is an approximation of a range.

These USGS olivine can be divided into two groups as demonstrated in Figure 1: (a) they have the same grain size ( $<60\ \mu\text{m}$ ) with increasing Fo#; (b) they have the same Fo# with increasing grain size ( $60\ \mu\text{m}$  to  $165\ \mu\text{m}$ ). Usually, laboratory spectra with larger grain size ( $>45\ \mu\text{m}$ ) are more similar to the natural mineral spectra than the small grain size (Clénet et al. 2011). Making it with the same grain size, with powder size  $<60\ \mu\text{m}$ , the spectral reflectance

increases and band depth decreases with increasing Fo# (decreasing  $\text{Fe}^{2+}$ ). Obviously, as the iron abundance increases, the band center position of the  $1.0\ \mu\text{m}$  absorption band shifts toward longer wavelength. In addition, the particle size also affects the spectral reflectance and band shape (Salisbury & Eastes 1985; Salisbury & Wald 1992). The spectral absorption features of forsterite shift toward longer wavelengths when the grain size increases. When band saturation in very large grain sizes occurs, determination of the band center will become complicated.

## 2.2 Using MGM to Deconvolve Olivine Spectra

In MGM, natural logarithm of each spectral reflectance is modeled as

$$\ln [R(\lambda)] = F(\text{cont}) + \sum_{i=1}^N S_i \cdot \exp \left[ -\frac{(\lambda^{-1} - \mu_i^{-1})^2}{2\sigma_i^2} \right], \quad (1)$$

where  $\lambda$  is the wavelength,  $R(\lambda)$  is the reflectance at wavelength  $\lambda$ ,  $S$  is the band strength,  $\mu$  is the band center,  $\sigma$  is the band width and  $N$  is the number of bands.  $F(\text{cont})$  is a function of the continuum in wavenumber space.

The MGM is not very dependent on pre-hypothesis of spectral components, but band absorption analysis needs to be done with suitable caution to ensure that the absorption has physical significance. In the olivine spectra, there are two inflection regions near 700 and 1800 nm, and a wide absorption near  $1\ \mu\text{m}$  region. The Gaussian curves in Figure 2 indicate that there are three absorptions (870 nm, 1050 nm and 1250 nm, respectively, which are assigned to transitions of  $\text{Fe}^{2+}$  in the M1–1, M2 and M1–2 sites of olivine) in this region (Sunshine & Pieters 1998). The initial parameters based on prior knowledge of the mineral spectral absorption can be set in advance when running the MGM code. Therefore, the number of Gaussian curves to be included in the model directly depends on the number of absorption bands present in the spectrum. In order to elaborate on this model, there are four basic characteristics significant for interpreting and exploiting the MGM, as illustrated in Figure 2. They are: (1) band center (the central location of each absorption feature); (2) band width (typically described as the full width at half maximum (FWHM) in the independent reflectance spectrum curve); (3) band strength (the band intensity in natural logarithmic reflectance space); and (4) continuum (a mathematical function used to describe the prominence for a particular spectral absorption feature in the analysis) (Sunshine & Pieters 1993; Clark & Roush 1984).

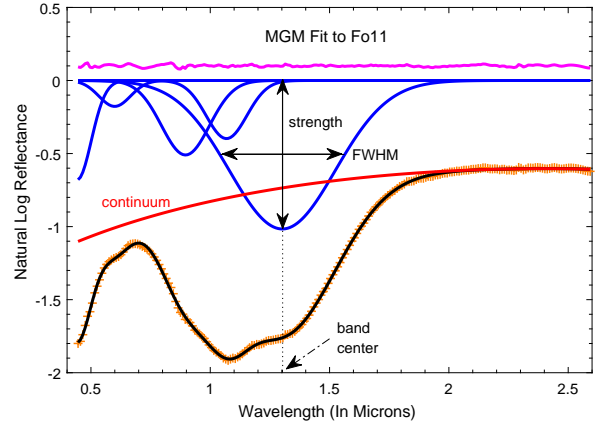


**Fig. 2** Four significant characteristic parameters for MGM. In this figure, the spectral data (Sample ID: KI3005, Fo11) are from the USGS spectral library. The orange “+” symbols are the logarithm reflectance data of KI3005. The blue lines are Gaussian curves fit to the reflectance data. The red line represents a type of continuum used in the MGM. The black line is the fitting result representing the Gaussian curves plus the continuum. The pink line signifies the residuals (original data minus modeled Gaussian fitting result). For the sake of clarity, the residuals are shifted by +0.1 on the ordinate.

## 2.3 Different Continuum Removal Methods

The slope of the continuum is variable, which consists of a number of factors such as grain size, viewing geometry, space weathering, temperature, etc. The variable continuum is a barrier for quantitative analysis of spectral diagnostic absorption features (Isaacson et al. 2011). To quantify the absorption band features, it is necessary to remove the continuum from the spectral curve, however, the physical significance of the continuum is not thoroughly understood yet (Clark et al. 2003; Clénet et al. 2011). Accurately modeling a suitable “continuum” with superimposed absorptions is not easy but crucial for analyzing the spectroscopic data with the MGM.

In the MGM program, users can set clear continuum polynomial parameters. In order to compare the relative absorption band intensity and study the effect of the continuum removal method (C for short) on the MGM deconvolution, four different types of continuum removal methods in wavelength space are utilized in this article to get the olivine diagnostic spectral features:

1. Flat line continuum removal method (Method F for short)

Use the logarithm of the max reflectance values and one additional model parameter for offset as a flat continuum to remove in wavelength space.

$$C(\lambda) = \ln(\text{MAX}(R)) + c_0. \quad (2)$$

$R$  = reflectance,  $\lambda$  = wavelength,  $c_0$  = constant.

**Table 1** Olivine Spectra Selected for Comparing Continuum Removal Methods in this Study

USGS Spectral Library			RELAB Spectral Database					
Sample ID	Size ( $\mu\text{m}$ )	Fo#	Sample ID	Size ( $\mu\text{m}$ )	Fo#	Sample ID	Size ( $\mu\text{m}$ )	Fo#
KI3005	< 60	11	DD-MDD-087	< 45	80	DD-MDD-115	< 45	89.5
KI3377	< 60	19	DD-MDD-088	< 45	75	DD-MDD-116	< 45	70
KI3291	< 60	30	DD-MDD-089	< 45	70	DD-MDD-046	< 45	0
KI4134	< 60	41	DD-MDD-090	< 45	65	DD-MDD-045	< 45	10
KI3188	< 60	51	DD-MDD-091	< 45	60	DD-MDD-044	< 45	20
KI3189	< 60	60	DD-MDD-092	< 45	55	DD-MDD-043	< 45	30
KI3054	< 60	66	DD-MDD-093	< 45	50	DD-MDD-042	< 45	40
GDS70.d	< 60	91	DD-MDD-094	< 45	40	DD-MDD-041	< 45	50
GDS71.b	< 60	92	DD-MDD-095	< 45	30	DD-MDD-040	< 45	60
GDS70.e	< 30	91	DD-MDD-096	< 45	20	DD-MDD-039	< 45	70
GDS70.c	< 70	91	DD-MDD-097	< 45	10	DD-MDD-038	< 45	80
GDS70.b	< 115	91	DD-MDD-098	< 45	0	AG-TJM-008	< 45	90
GDS70.a	< 165	91						

The origins of the samples involved in this paper are different. Olivine in USGS Spectral Library is terrestrial olivine in nature, and its Fo# are accurately calculated to the unit digit with the chemical composition analysis (e.g., for KI3054, Fo66 is an approximation of the exact number 65.53). Olivine in RELAB Spectral Database represents synthetic samples, as described by Dyar et al. (2009), and its Fo# is an approximation of a range (e.g., DD-MDD-091, Fo60 is an approximate number ranging from 53 to 64).

2. Oblique line continuum removal method (Method O for short)

Use the logarithm of first-order trend line as a continuum to remove in wavelength space.

$$C(\lambda) = \ln(c_0 + c_1\lambda). \quad (3)$$

$\lambda$  = wavelength,  $c_0, c_1$  = constants.

3. Polynomial curve continuum removal method (Method P for short)

Use the logarithm of second-order polynomial curve as the continuum to remove in wavelength space.

$$C(\lambda) = \ln(c_0 + c_1\lambda + c_2\lambda^2). \quad (4)$$

$\lambda$  = wavelength,  $c_0, c_1, c_2$  = constants.

4. Energy-wavelength polynomial continuum removal method (Hiroi et al. 2000) (Method E for short). Use the energy-wavelength polynomial as the continuum to remove in wavelength space.

$$C(\lambda) = \frac{c_0}{\lambda} + c_1 + c_2\lambda. \quad (5)$$

$\lambda$  = wavelength,  $c_0, c_1, c_2$  = constants.

Flat line, oblique line and polynomial curve continuum removal methods are commonly utilized in the MGM deconvolution. Hiroi et al. (2000) developed Method E for deconvolving the reflectance spectra of lunar soils. Figure 3 displays an example of MGM fit to fayalite (Fo11) using the above mentioned four continuum removal methods.

## 2.4 MGM Parameters and Initialization

Following the previous explanation in Sections 2.2 and 2.3, each Gaussian curve must be initialized with three parameters (band center, band width and band strength) and each parameter corresponds to a  $2\sigma$  uncertainty. Likewise, the continuum must be initialized as a certain type with the corresponding  $2\sigma$  uncertainty for each parameter. In addition to the  $1\mu\text{m}$  region, sometimes, another two or more Gaussians at the short wavelength region, and one or more Gaussians at the long wavelength region are also needed to obtain physically realistic modeling to initialize the MGM. The former is used to model the strong large absorption of charge transfer near the ultraviolet region and weak absorption near  $0.6\mu\text{m}$  (Clénet et al. 2011), and the latter is utilized to model the absorption of atmospheric water in the long-wavelength region (Dyar et al. 2009).

The transmission spectra of olivine have been studied in detail by Burns (1970). In his work, spectra from all three ( $\alpha, \beta, \gamma$ ) crystallographic optical orientations were examined as a function of compositions. He deconvolved each of the  $\alpha, \beta, \gamma$  polarized spectra into three absorption bands. In the  $\alpha$  and  $\beta$  polarized spectra, M1–1 band and M1–2 band contribute most strongly to the spectra, and M2 band has little or no contribution to the spectra. Whereas, the M2 band is most intense in the  $\gamma$  orientation, and form a narrow and sharp curve. However, reflectance spectra of pulverized samples are different from the polarized transmission spectra of single crystals in that the former ones include scattering contributions from randomly orientated micro-crystals. The shape of reflectance spectra is more similar to  $\alpha$  and  $\beta$  polarized spectra, but not the sharp curve of the  $\gamma$  polarized spectra. To deconvolve olivine spectral absorptions more accurately, the research presented here initializes the intensity of M2 to about half of M1–2.

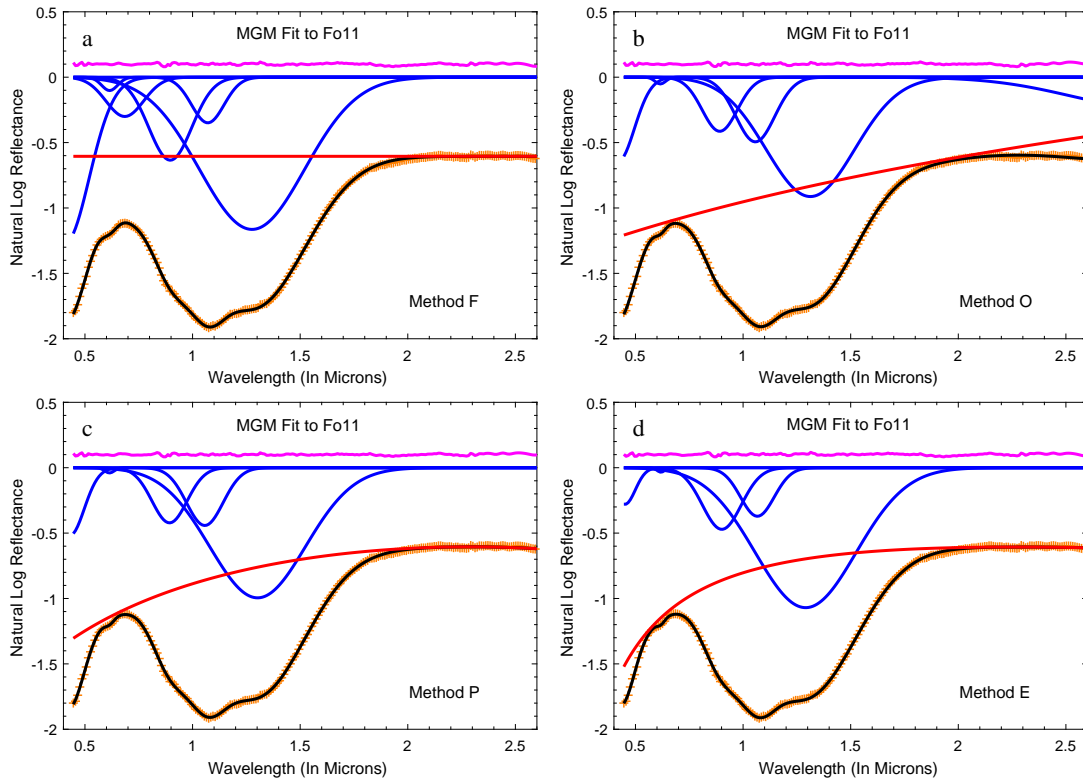


**Fig. 3** Olivine (Fo11) spectral deconvolution results from four continuum removal methods of MGM. Panels a, b, c and d represent the four methods of F, O, P and E, respectively. a: flat line continuum without slopes was used to match the flat spectra in the long wavelength regions for simplicity. b: oblique line continuum tangent to the two inflection regions on both sides of the absorption region. c: quadratic polynomial curve continuum describes the general spectral trend. d: energy-wavelength polynomial continuum describes the general spectral trend.

The relative strength shifts with the variations of olivine Fo#. Although this relationship is less useful for compositional analysis, it should be also of concern as mentioned in [Sunshine & Pieters \(1998\)](#). A series of tests of the MGM modeling has driven us to set appropriate Gaussian parameters and determine the uncertainty of 50 nm for the band center, 50 nm for the band width and within 30% for the band strength. For poor quality spectra, it can also reduce the  $2\sigma$  uncertainty to model the data accurately. Continua of Methods O, P and E were modeled as closely as possible to the two inflection regions near 700 nm and 1800 nm. The parameters of the continuum are variable with different selected methods, and we set an uncertainty within 30% for each continuum parameter.

## 2.5 Space Weathering Simulations of Olivine Grains

In order to test how MGM may work for samples that have experienced simulated space weathering, we re-analyzed the reflectance spectra of olivine grains (less than 45  $\mu\text{m}$ ) irradiated by a pulse laser with different intensity levels ([Yang et al. 2017](#)). The detailed experimental procedures can be found in [Yang et al. \(2017\)](#) and the following is a brief summary:

In order to study the effects of space weathering on olivine diagnostic spectral features, some natural pure olivine granules were collected and ground into powder (less than 45  $\mu\text{m}$ ) as the sample. A wet chemistry method was followed to analyze the major contents of olivine elements and its Mg-number is Fo89.8. Olivine powders were baked with a dry oven at 120° C for more than 5 hours to remove any moisture in the samples, and then the dry samples were placed in aluminum holders in a vacuum chamber under a pressure of  $10^{-3}$  Pa for pulsed laser irradiation. By varying the pulse energy and irradiation time, this approach could simulate different degrees of weathering.

We obtained a total of six olivine samples with varying degrees of weathering, including the original unirradiated one. A continuum nanosecond pulsed laser was operated to simulate the micrometeorite bombardment process. The pulse energy was set as 25 mJ pulse<sup>-1</sup>, and different irradiation times were applied for these samples to simulate varying degrees of micrometeorite bombardments. Before and after irradiations, VNIR reflectance spectra of these olivine samples were measured with a Bruker Vertex 70 Fourier transform infrared spectrometer. The transmission electron microscope (TEM) images of irradiated olivine show the presence of  $\text{npFe}^0$ .

### 3 RESULTS AND DISCUSSIONS

#### 3.1 Different Continua on Spectral Deconvolution

According to the definition of the MGM, Gaussian fitting of the spectral curve needs to be processed by the continuum removal method. Flat line continuum (Method F) (Fig. 4) is the original choice by Sunshine & Pieters (1998). This method should be applied with caution for spectral deconvolution, due to the fact that such flat spectra in the near-infrared (NIR) regions are almost nonexistent in mafic rocks, mixed minerals or lunar regolith. Compared with the widely used continuum removal method developed by Clark & Roush (1984), this method will significantly overstate the absorption strength of the slope spectra in the ultraviolet and visible regions, when the continuum is far from the curve of the visible region.

Oblique line continuum corresponds to Method O, which relies on the continua to contact the two inflection regions near 700 nm and 1800 nm. Cases in Figure 5 demonstrate that this method will significantly overestimate the NIR region ranging from 2.0  $\mu\text{m}$  to 2.6  $\mu\text{m}$ . Actually, there is no significant absorption feature in this region. Isaacson et al. (2011) employed a similar continuum removal method to study the lunar olivine-dominated spectra in an individual absorption region. It takes some unrealistic physical modeling to fit the spectra in the longer wavelength region ( $>2.0 \mu\text{m}$ ).

Polynomial continuum corresponds to Method P, the logarithm of a second-order polynomial curve, and was used as the continuum to be removed in the MGM (as shown in Fig. 6). Sunshine & Pieters (1998) applied this method to fit an olivine-rich asteroid spectrum. However, they did not restrict the parameters of continuum so that a small range of variable Fo# was accepted. With this method, the overall shape of the continuum can describe the general spectral trend well.

For Method E, the energy-wavelength polynomial continuum does not need to be converted to natural logarithm space, because it was originally defined in natural logarithm space (Fig. 7). This method is similar to a combination of Method O and Method P. Olivine diagnostic spectral feature (700~1800 nm) can be described well, but sometimes it may underestimate absorption in the visible region.

#### 3.2 Variations of the Diagnostic Band Center

In order to reveal the olivine composition from the MGM deconvolution results obtained using different continuum removal methods, it is essential to recalculate the three regression trend lines established by Sunshine & Pieters (1998). In addition, the position of the composite band center is also widely utilized to determine the composition

of olivine or pyroxene. Figure 8 depicts the variations of the olivine diagnostic band center position with their regression lines and the composite band centers. Table 2 displays the linear regression equations of the three diagnostic band centers, the composite band centers and the residuals. Comparison of the results of the four continuum removal methods and the trend lines of the composite band centers are featured in Figure 9.

As expected, with each method, olivine diagnostic band centers move toward longer wavelength with increasing iron content (decreasing Fo#), and the two M1 band centers move faster than M2. The trend lines of M1–1 and M2 bands obtained by Method F are very close to those in Sunshine & Pieters (1998), but there are some changes in the M1–2 band, which may be due to the fact that we considered more sample data and/or a different offset. In contrast to Method F, the linear regression equation system of the other three methods all demonstrate that the slope rates are less than the corresponding values in Sunshine & Pieters (1998). As discussed in Sections 2.3 and 3.1, different continua in the MGM deconvolution will significantly influence the location and distribution of the band center, especially the trend of M1–1 and M2. With Method O, Method P and Method E, the trend lines of M2 band center position appear to be shifted by a few nanometers toward short wavelengths with a smaller slope than the results of Sunshine & Pieters (1998).

We note that the spectral curve becomes flat with increased Fo#, especially when Fo#  $>90$  (Fig. 1). In addition, deconvolution results always shift a little bit toward longer wavelength when Fo#  $>80$ . The absolute spectral strength of olivine will decrease and spectral curve will become flattened with decreasing iron content. Therefore, if the absorption is too weak, the interpretation of the deconvolution results should be taken cautiously.

For the MGM deconvolution of the continuum removal method, Figure 8 and Table 2 show the linear regression equations and residuals. Method F is the original choice by Sunshine & Pieters (1998). The trend lines of M1–1 and M2 in this paper are almost the same as those in Sunshine & Pieters (1998), but the centers of M1–2 are more dispersed, which indicates that this method may be not suitable for continuum removal.

Method O is a simple and feasible method, but compared with other methods, the sum of residuals of all three diagnostic band centers is the largest. Moreover, the oblique line continuum will significantly overestimate the NIR region longer than  $\sim 2.0 \mu\text{m}$ . As a result, it needs to add some Gaussian curves without physical significance to fit the spectral curves. Fortunately, the diagnostic spectral characteristics of olivine do not exceed this region, hence we can restrict the spectral range to  $\sim 0.6 \mu\text{m} < \text{wavelength} < \sim 1.8 \mu\text{m}$  to study the olivine composition. However, we

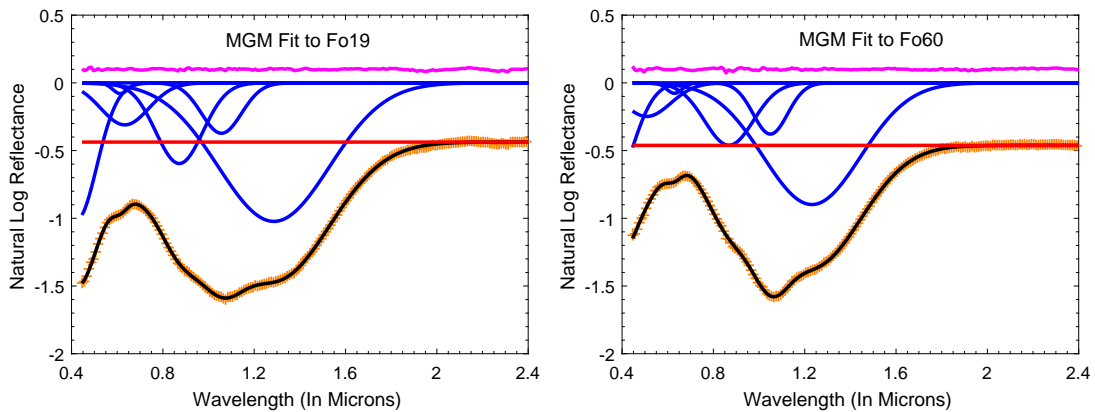


**Fig. 4** Example of different Fo# olivine spectral deconvolution results from flat line continuum removal method (Method F) of MGM.

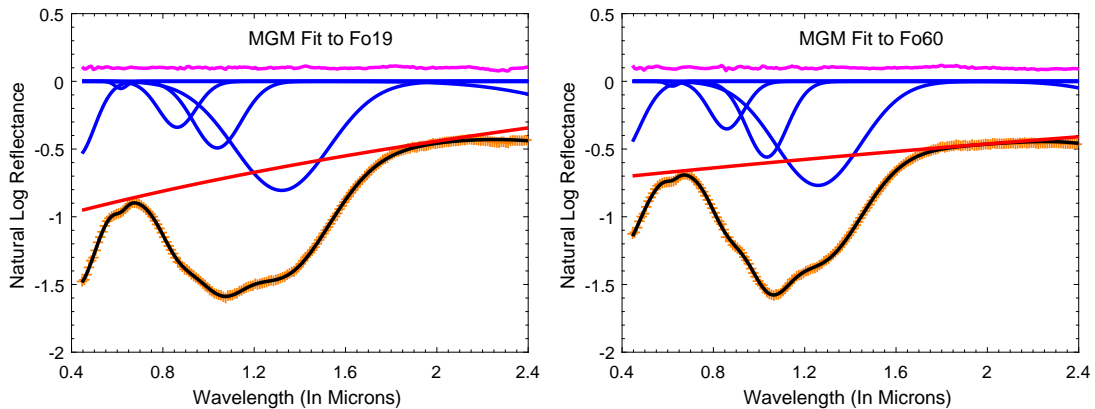


**Fig. 5** Example of different Fo# olivine spectral deconvolution results from oblique line continuum removal method (Method O) of MGM.

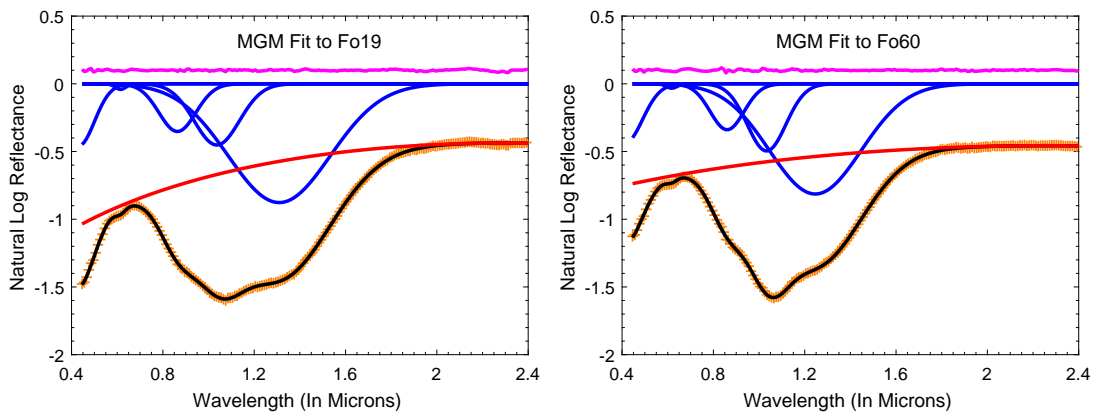


**Fig. 6** Example of different Fo# olivine spectral deconvolution results from second-order polynomial continuum removal method (Method P) of MGM.

still do not recommend this approach due to its large residuals.

Method P is commonly implemented in MGM deconvolution. With appropriate parameters, the overall shape of the smooth curved continuum can describe the general spectral trend well. Compared with other methods,

Method P is also a simple and effective method. More importantly, this method does not need to initialize the Gaussian curves that do not have physical significance.

Method E was developed for deconvolving the reflectance spectra of lunar soils. It is not widely used in MGM deconvolution, maybe because it requires complex

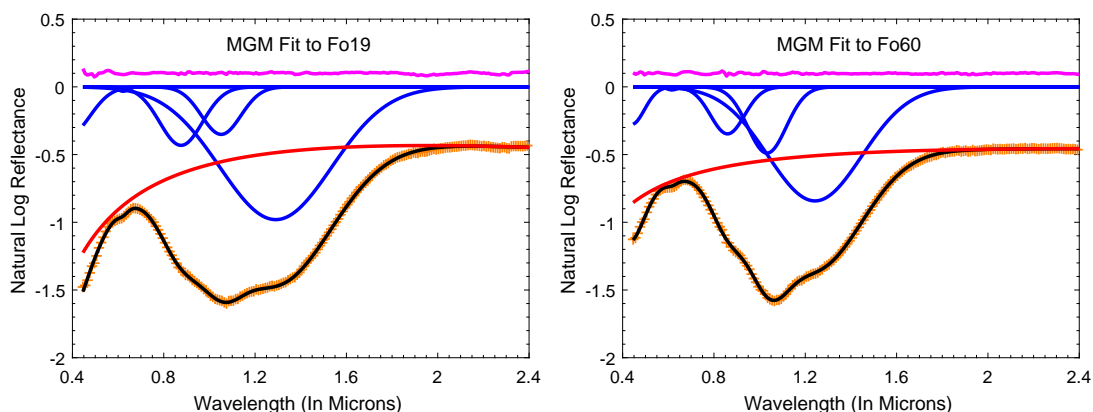


**Fig. 7** Example of different Fo# olivine spectral deconvolution results from energy-wavelength polynomial continuum removal method (Method E) of MGM.

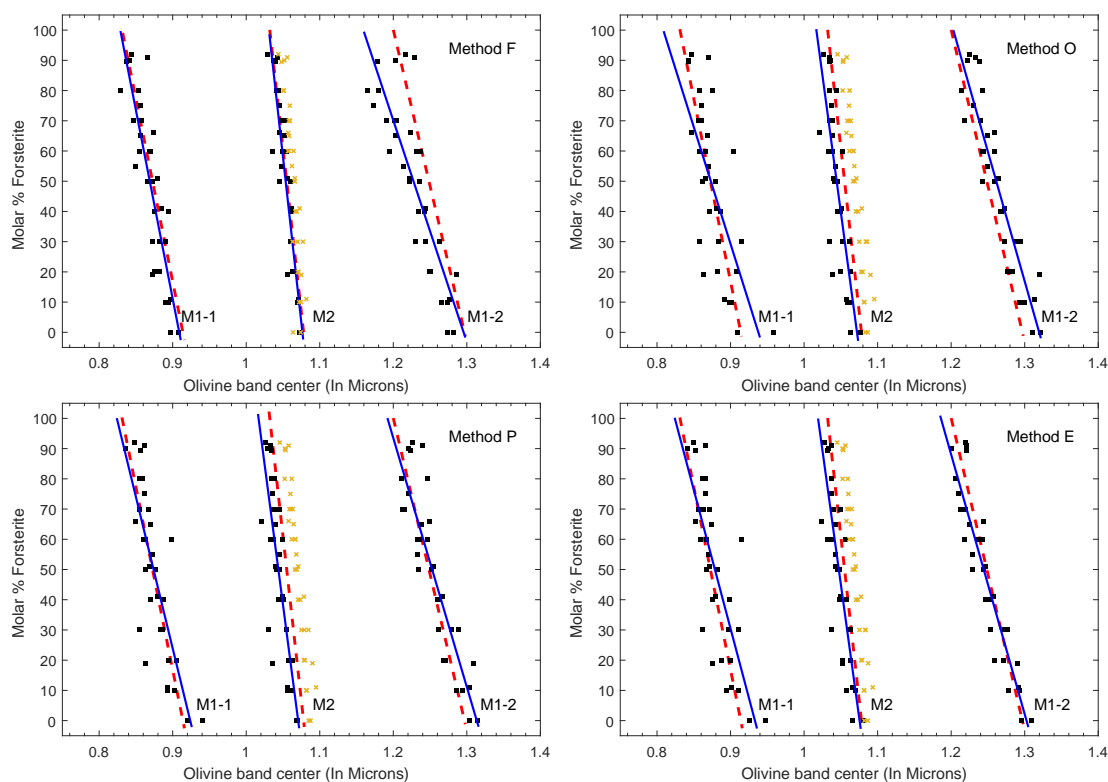


**Fig. 8** Band centers of the olivine spectral deconvolution results from four continuum removal methods of MGM are compared with the trends defined by Sunshine & Pieters (1998). For this figure, *black square symbols* represent the deconvolution results obtained in this paper, *solid blue lines* signify these result trend lines and *red dashed lines* correspond to the trend lines defined by Sunshine & Pieters (1998). *Yellow crosses* mark the composite band centers.

**Table 2** Linear Regression Equations of the Three Diagnostic Band Centers with Different Methods

Method	M1-1			M2			M1-2			Composite Band		
	a	b	residual	a	b	residual	a	b	residual	a	b	residual
F	-1247.4	1133.8	79.52	-2195.9	2363.7	64.44	-733.42	950.25	80.47	-2691.8	2911.7	77.42
O	-773.65	725.53	103.97	-1810.1	1940.3	96.70	-856.71	1130.6	59.06	-2131.8	2329.9	56.81
P	-1002.2	925.89	94.48	-1857.4	1988.6	92.83	-823.82	1082.1	68.71	-2170.9	2371.5	51.72
E	-918.19	856.8	96.18	-1770.7	1904.3	84.61	-859.06	1118.9	54.70	-2215.4	2418.0	51.59

The expression of the linear regression equation is:  $Fo\# = a*\lambda + b$ , where a and b are variable coefficients;  $\lambda$  is wavelength in microns.

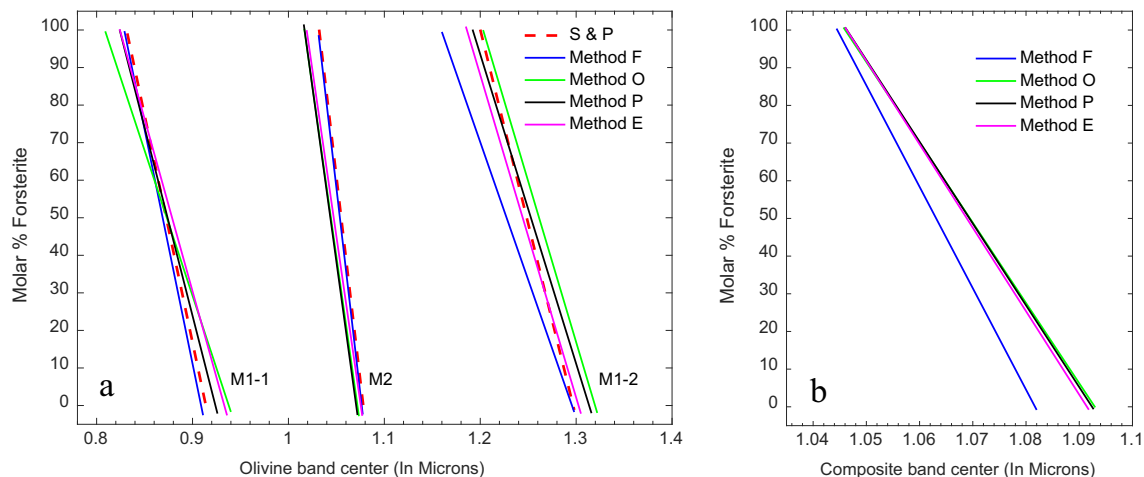


**Fig. 9** Comparison of the results of the four continuum removal methods and the trend lines of the composite band centers obtained by four continuum removal methods. S&P represents the trend lines defined by [Sunshine & Pieters \(1998\)](#).

and harsh initialization parameters. Furthermore, with the iterative parameters of this polynomial continuum, the stochastic non-linear inverse algorithm sometimes makes the new parameters worse than the old do. In this case, the deconvolution result is untrustworthy. This method requires manual reexamination to make sure the result is correct, which will introduce more labor requirements. In view of these, Method E is not suitable for defining the continuum for plenty of remote sensing data.

In Figure 9(a), a comparison of the results obtained by the four continuum removal methods and the original method is clearly depicted. What is more, in Figure 9(b), the trend lines of the composite band centers of Methods O, P, and E are close, but the trend line of Method F is significantly different from others. Moreover, [Clark & Roush \(1984\)](#) pointed out that implementing a flat continuum to calculate the maximum absorption position of the reflectance spectrum is incorrect, which also indicates that the trend lines in [Sunshine & Pieters \(1998\)](#) should be used with caution. Clearly, in terms of operability and practicality, Method P, the logarithm of a second-order polynomial continuum, may be the best choice in this paper for further research.

### 3.3 Comparison between Method P and Sunshine & Pieters (1998)

It is worth noting that the trend lines of the diagnostic band centers exhibit some difference from those defined by [Sunshine & Pieters \(1998\)](#) and Method P. The band center and deviation obtained by these two methods with Fo# changing in order are shown in Table 3. The deviations indicate that the corresponding band centers are quite different between the deconvolution results of Method P and [Sunshine & Pieters \(1998\)](#). Evidently, the deviation of the two methods on M1–1 band is more than  $-5\sim 8$  nm, even

though the band centers display a well-defined linear trend. The deviations on M2 and M1–2 are more than  $-14$  nm and  $-5\sim 14$  nm respectively. Such a wide shift in the band center will require careful handling of deconvolution results.

In fact, Method P, the logarithm of a second-order polynomial continuum, matches the overall shape of the spectrum well, and is a popular choice now. In order to study the difference in the two different trend lines and estimation results, we also calculated the Fo# and correction which was obtained from the two regression equations defined by Method P and [Sunshine & Pieters \(1998\)](#) while the band centers were altered in order. Table 4 indicates that the estimated results of the two different trend lines are quite different. It will overestimate more than 7 mol% for forsterite and underestimate more than 9 mol% for fayalite on M1–1 band if we use the regression equations defined by [Sunshine & Pieters \(1998\)](#). Similarly, it will overestimate more than 4 mol% for forsterite and underestimate more than 14 mol% for fayalite in M1–2 band. Considering that the estimation of mafic mineral abundance and chemical composition difference is between 5%  $\sim$  10%, the difference between the results of these two methods is acceptable. Conversely, as for M2 band, the prediction results of these two methods vary greatly, and it will overestimate the Fo# by about 15 to 30 from fayalite to forsterite. There is a need to determine which method is better.

### 3.4 Validation and Application: Analysis of Olivine-dominated Meteorite Spectra

This research relies on olivine-dominated meteorite spectra to test Method P and its trend lines described above. Brachinites are unshocked equigranular igneous material, which belongs to differentiated ultramafic achondrites but not a part of primitive achondrites ([Nehru et al. 1983, 1992; Mittlefehldt et al. 2003](#)), and arguably may

**Table 3** Linear Regression Equations of the Three Diagnostic Band Centers with Method S&P and Method P

Fo#	M1–1 (nm)			M2 (nm)			M1–2 (nm)		
	S&P	Method P	Deviation	S&P	Method P	Deviation	S&P	Method P	Deviation
10	905.6	913.9	8.3	1073.4	1065.3	–8.2	1287.2	1301.4	14.2
20	897.4	903.9	6.5	1068.8	1059.9	–9.0	1277.5	1289.2	11.7
30	889.1	893.9	4.8	1064.2	1054.5	–9.7	1267.8	1277.1	9.3
40	880.8	883.9	3.1	1059.6	1049.1	–10.5	1258.2	1265.0	6.8
50	872.6	874.0	1.4	1055.0	1043.7	–11.3	1248.5	1252.8	4.3
60	864.3	864.0	–0.3	1050.4	1038.3	–12.1	1238.8	1240.7	1.9
70	856.0	854.0	–2.0	1045.8	1032.9	–12.9	1229.1	1228.5	–0.6
80	847.8	844.0	–3.7	1041.2	1027.6	–13.7	1219.4	1216.4	–3.0
90	839.5	834.1	–5.5	1036.6	1022.2	–14.5	1209.8	1204.3	–5.5

S&P represents the trend lines in [Sunshine & Pieters \(1998\)](#). Deviation is equal to the result of Method P minus S&P.

**Table 4** Different Estimated Results (Fo#) and Corrections between the Two Regression Equations Defined by Method S&P and Method P

Band Center	Fo# (M1–1)			Band Center	Fo# (M2)			Band Center	Fo# (M1–2)		
	S&P	Method P	Correction		S&P	Method P	Correction		S&P	Method P	Correction
0.830	101.5	94.1	–7.5	1.030	104.5	75.5	–29.0	1.210	89.8	85.3	–4.5
0.840	89.4	84.0	–5.4	1.035	93.6	66.2	–27.4	1.220	79.4	77.0	–2.4
0.850	77.3	74.0	–3.3	1.040	82.7	56.9	–25.8	1.230	69.1	68.8	–0.3
0.860	65.2	64.0	–1.2	1.045	71.8	47.6	–24.2	1.240	58.8	60.6	1.8
0.870	53.1	54.0	0.9	1.050	60.9	38.3	–22.6	1.250	48.4	52.3	3.9
0.880	41.0	44.0	2.9	1.055	50.1	29.0	–21.0	1.260	38.1	44.1	6.0
0.890	28.9	33.9	5.0	1.060	39.2	19.8	–19.4	1.270	27.8	35.8	8.1
0.900	16.8	23.9	7.1	1.065	28.3	10.5	–17.9	1.280	17.4	27.6	10.2
0.910	4.7	13.9	9.2	1.070	17.4	1.2	–16.3	1.290	7.1	19.4	12.3
0.920	–7.4	3.9	11.3	1.075	6.6	–8.1	–14.7	1.300	–3.3	11.1	14.4

Olivine band centers are in microns. S&P represents the trend lines in [Sunshine & Pieters \(1998\)](#). Olivine with an Fo# greater than 100 or a negative number does not exist.

have come from differentiated asteroids ([Mittlefehldt et al. 2003](#)). Based on their similarities in reflectance spectra, the A-type asteroids are believed to be olivine-dominated and the parent bodies of brachinites ([Nesvorný et al. 2009](#)). In this work, the spectra of meteorite Brachinite EET99402 with different grain sizes (RELAB sample ID: MT-JMS-088, MT-JMS-329, TB-TJM-058) were chosen as the examples to study its chemical composition. The average mineral compositions, major, minor and trace element contents of EET 99402 were analyzed by [Mittlefehldt et al. \(2003\)](#). They reported that when converted to weight percent, there are olivine 88.0%, high-Ca pyroxene 4.7%, plagioclase 6.1%, spinel 1.0% and troilite 0.1%. In addition, olivine has an average composition of Fo64.2.

The spectra of EET 99402 were deconvolved by MGM with continuum removal Method P, which aims to determine whether the prediction results of olivine compositions are consistent with their known chemistry. Figure 10 displays the deconvolution results, while Table 5 lists the starting parameters used to initialize the spectra and final parameters obtained by MGM deconvolution. Furthermore, Figure 10(d) shows the predicted results of the three spectra of ETT 99402. The predicted Fo# of the three spectra are Fo60.3, Fo63.8 and Fo62.6, respectively, and the average value is Fo62.3. The estimated result is very close to its chemical component (Fo64.2), and it is

superior to  $\sim$ Fo60 which was calculated by [Sunshine et al. \(2007\)](#). This is probably because we included more samples with different grain sizes to make the estimates more accurate.

According to the comparison and discussion mentioned above, it should be mentioned that if we apply different continuum removal methods to deconvolve the spectrum with MGM, significantly different absorption band center positions will be produced. These band centers are crucial for studying the olivine composition (Fo#). Therefore, caution should be exercised for the regression equation obtained by unknown or different continuum removal methods.

Generally speaking, the optimal continuum removal method mainly depends on the overall shape of the spectral curve. For a single simple absorption band, we usually choose a simple flat or oblique tangent line as the continuum. The widely utilized cubic splines continuum in [Clark & Roush \(1984\)](#) is similar to the tangent line continuum removal method. When shifted to the logarithmic space of the reflectance, the oblique line will bend to have a little curvature at the short wavelength region. The physical significance of the continuum is not clear yet. If we do not want to increase the absorption bands without physical significance and excessively decrease the band intensity, the logarithm of a second-order polynomial continuum,

**Table 5** MGM Modeling Parameters of the Meteorite Brachinite EET99402 Spectra

Sample ID		MT-JMS-088		MT-JMS-329		TB-TJM-058	
Grain size		Fine powder		<45 $\mu\text{m}$		<125 $\mu\text{m}$	
Gaussian fitting parameter		Starting parameters	Final parameters	Starting parameters	Final parameters	Starting parameters	Final parameters
Continuum	Parameter 1	$3.50 \times 10^{-1}$	$3.37 \times 10^{-1}$	$3.30 \times 10^{-1}$	$3.54 \times 10^{-1}$	$1.40 \times 10^{-1}$	$1.38 \times 10^{-1}$
	Parameter 2	$5.00 \times 10^{-5}$	$5.14 \times 10^{-5}$	$5.00 \times 10^{-5}$	$1.97 \times 10^{-5}$	$5.00 \times 10^{-5}$	$4.51 \times 10^{-5}$
	Parameter 3	$-2.00 \times 10^{-8}$	$2.08 \times 10^{-8}$	$-1.50 \times 10^{-8}$	$6.06 \times 10^{-9}$	$-1.50 \times 10^{-8}$	$-1.29 \times 10^{-8}$
Band 1	Center	300	292.6	300	295.2	300	323.3
	FWHM	160	110.8	100	109.0	160	184.7
	Strength	-1.0	-1.21	-1.0	-1.36	-1.0	-1.04
Band 2	Center	400	349.6	400	374.7	480	480.4
	FWHM	200	250.9	100	222.6	100	97.5
	Strength	-0.3	-0.51	-0.3	-0.44	-0.4	-0.26
Band 3	Center	620	653.5	620	628.9	620	621.5
	FWHM	70	75.3	70	49.2	70	63.7
	Strength	-0.02	-0.0198	-0.02	-0.0188	-0.02	-0.0198
M1-1	Center	870	863.7	870	863.1	870	862.3
	FWHM	180	183.7	180	168.8	180	173.8
	Strength	-0.1	-0.12	-0.1	-0.11	-0.2	-0.24
M2	Center	1050	1041.4	1050	1039.4	1050	1036.1
	FWHM	200	184.0	200	187.9	200	198.4
	Strength	-0.25	-0.23	-0.25	-0.21	-0.35	-0.41
M1-2	Center	1250	1232.8	1250	1225.2	1250	1238.4
	FWHM	400	384.8	400	412.2	350	401.1
	Strength	-0.25	-0.24	-0.22	-0.24	-0.5	-0.50
Root Mean Square Error		$3.88 \times 10^{-3}$		$3.23 \times 10^{-3}$		$5.55 \times 10^{-3}$	

Band center and FWHM are in microns. Final parameters listed in this table are approximations rather than exact values.

which can match the overall shape of the varied spectral curves, may be the best choice.

### 3.5 Application of MGM in Space Weathering Analysis

#### 3.5.1 Reflectance spectra of irradiated olivine

Based on the optimized MGM method mentioned above for estimating olivine composition, the spectral characteristics of olivine subjected to space weathering simulated in the laboratory were studied. The VNIR reflectance spectra of the samples with varied laser irradiation degrees as well as the original one are plotted in Figure 11(a), while the same spectra normalized at 700 nm are shown in Figure 11(b).

After irradiation, those diagnostic spectral features turned weaker and shallower. As the amount of irradiation increases, absorption intensity and albedo of the visible region (we chose the reflectance value at 700 nm) decreases faster than the NIR region (we chose the reflectance value at 1800 nm), the behaviors of which redden the spectra. It is in accordance with lunar-style space weathering (Gaffey 2010). According to the methods described above, Method F and Method O do not apply to the reflectance spec-

tra of irradiated olivine. However, as mentioned above, Method P and Method E can be used for deconvolving the reflectance spectra of lunar soils. So, these two continua removal methods will be applied to study the reflectance spectra of irradiated olivine.

#### 3.5.2 Effects of space weathering on olivine diagnostic spectral features

The absorption center of olivine diagnostic spectra is near 1050 nm, and the edges of the wings are near 700 nm and 1800 nm as stated in Section 3.1. In order to quantify the variation of the olivine spectral curve in space weathering, we defined a function to characterize the stability of the spectral diagnostic features

$$SSDF_{\text{olivine}} = \frac{R_{700} - R_{1050}}{R_{1800} - R_{1050}}, \quad (6)$$

where  $SSDF_{\text{olivine}}$  is an abbreviation for stability of the spectral diagnostic features of olivine;  $R_{700}$ ,  $R_{1050}$  and  $R_{1800}$  represent the reflectance or albedo at 700 nm, 1050 nm and 1800 nm, respectively.

As  $SSDF_{\text{olivine}}$  does not depend on the absolute reflectance of the spectrum, relative reflectance spectrum is also applicable, especially the telescope spectra, which

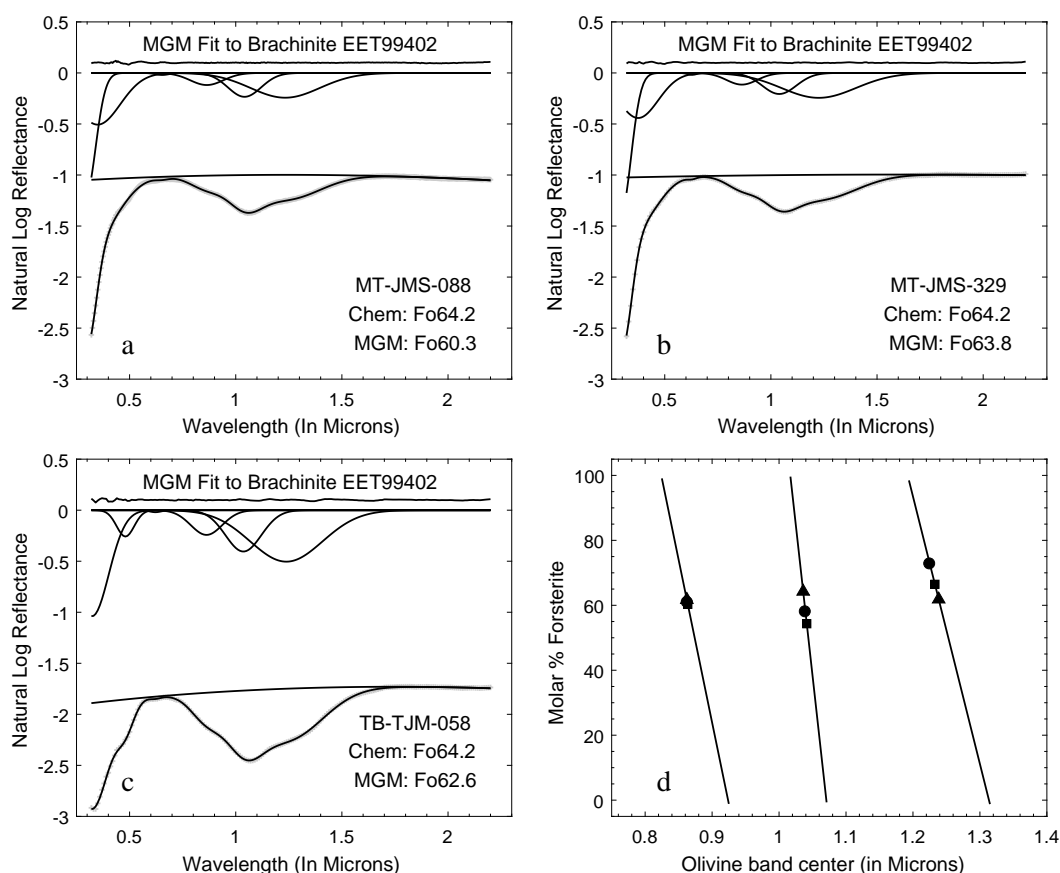


**Fig. 10** MGM fit to meteorite Brachinite EET99402 with Method P and prediction of the mole fraction of Fo#. Panels a, b and c are the MGM deconvolution results of Brachinite EET99402 spectra. Panel d: *solid lines* are the regression equations of Method P; *black squares, circles and triangles* represent the predicted Fo# of MT-JMS-088, MT-JMS-329 and TB-TJM-058, respectively.

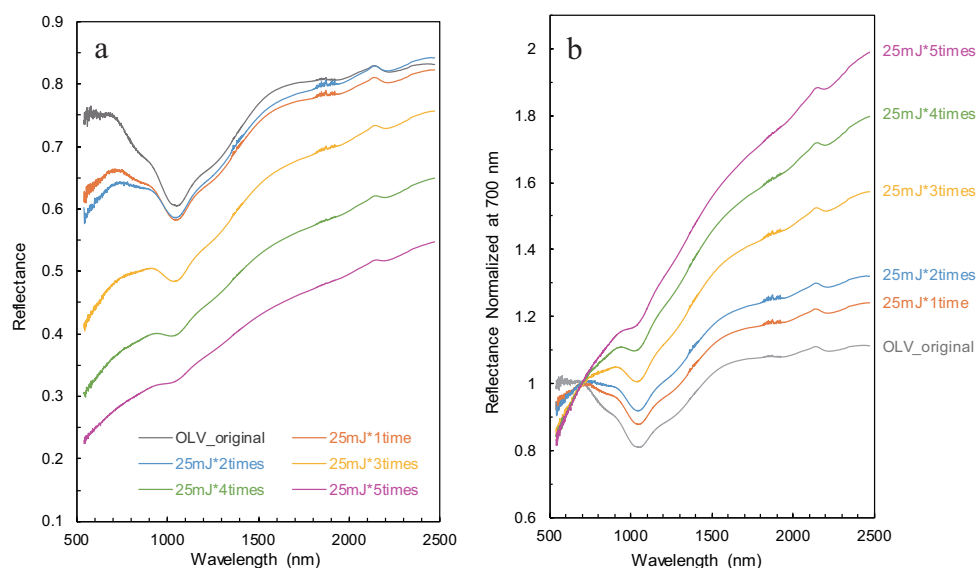


**Fig. 11** VNIR reflectance spectra and normalized spectra of olivine samples before and after irradiation. Panel a: all spectra are measured relative to a Spectralon standard with 99% nominal reflectance. Panel b: the reflectance spectra of olivine samples normalized at 700 nm.

makes Equation (6) more accurate and practical when studying space weathering. Table 6 lists parameters characterizing the VNIR spectral curves of olivine before and after irradiations. As the amount of radiation increases, the degree of spectral reddening increases and the stability of spectral diagnostic features decreases.

To quantify the effects of pulsed laser irradiation on olivine spectra, these experimental spectra were firstly smoothed using the Savitzky-Golay (SG) filter procedure (Savitzky & Golay 1964). MGM with the logarithm of a second-order polynomial continuum removal method (Method P) and an energy-wavelength polynomial continuum removal method (Method E) was employed to deconvolve the olivine spectra measured above. However, Method E demonstrates the instability of the algorithm and the complexity of parameter settings during the deconvolution process as described at the end of Section 3.2. So, we cannot really recommend using this method to study space weathered spectra. However, the data results obtained by this method are still shown below. In addition, we limit the VNIR feature discussions in the spectral region 500~2000nm, because the spurious peak near 2140 nm caused by Spectralon absorption can confuse and complicate mineral identifications (Zhang et al. 2014). Figure 12 depicts the diagnostic spectral features of these irradiated olivine grains and the original one obtained by Method P, while Tables 7 and 8 provide the final MGM fitting parameters of these spectra obtained by Method P and Method E, respectively.

The three diagnostic band centers of the original olivine spectrum deconvolved by MGM with Method P are 844.6 nm, 1025.9 nm and 1197.9 nm, respectively, and the deconvolution results with Method E are 847.7 nm, 1027.9 nm and 1201.6 nm, respectively. It is worth pointing out that the predicted Fo# of these three band centers using the Method P regression equation in this paper are Fo79.4, Fo83.1 and Fo95.2, respectively, and the predicted Fo# results with Method E are Fo78.5, Fo84.2 and Fo86.6, respectively. The average numbers of these two methods are Fo85.9 with Method P and Fo83.1 with Method E, respectively. These are close to its chemical composition Fo89.8. However, applying the regression equation provided in Sunshine & Pieters (1998) with the deconvolution results of Method P will result in three inappropriate results, which are Fo83.9, Fo113.4 and Fo102.2, respectively. In addition, the average number is slightly larger than Fo99.8. Noticeably, when Fo# is greater than 100, the predicted result is unacceptable and the estimated results differ from the chemical composition by more than 10 (mol%). Therefore, care needs to be applied when considering the regression equation based on Sunshine & Pieters (1998).

Regarding space weathering, after irradiation, these diagnostic spectral features turned narrower and shallower, and the three parameters (band center, band width and band strength) of M1–1 band manifest the fastest change. The absorption features of M2 band are relatively stable. Band centers gradually become larger and band strength gradually reduce, until the spectral absorption characteristics become very weak. The absorption intensity of the M1–2 band decays faster than the M2 band. Compared with the original olivine spectrum, all diagnostic band centers of the irradiated olivine spectra shift towards longer wavelength. The data in Figure 13 were obtained using Method P. After irradiation, the band center offsets reach up to 24.7 nm, 14.5 nm and 25.9 nm, for M1–1, M2 and M1–2 bands, respectively. This will cause the estimated Mg-numbers to be reduced from Fo85.9 to Fo61.6, corresponding to a change of more than 24 mol% for forsterite (or fayalite) in these olivine compositions. This result is consistent with the findings in Fu et al. (2012). Method E exhibits the same trend as Method P but with different quantities. As a result, the predicted forsterite proportion on the space weathered asteroid surface based on telescopic spectra may be less than its actual chemical composition.

### 3.6 Estimating the Composition of A-type Asteroids (246) Asporina and (354) Eleonora

The regression equations based on the center of the olivine spectral features in this paper can be applied to estimate the surficial composition of olivine-dominated asteroids. However, the estimated chemical compositions can be changed by space weathering according to the above statement. Two A-type asteroids (246) Asporina and (354) Eleonora were chosen to study its possible mineralogical characterization. The VNIR spectra of (246) Asporina and (354) Eleonora (Fig. 14) were obtained from the website of Planetary Spectroscopy at MIT<sup>4</sup>. The telescopic spectrum of (246) Asporina is a good sample for this study. It is inferred to be an olivine rich asteroid based on the dominant broad absorption feature near 1.0 nm in its VNIR spectrum. Whereas, the reddened spectrum has been interpreted to be affected by space weathering that produce metal particles on the surface (Cruikshank & Hartmann 1984). The spectrum of (354) Eleonora is in a similar situation (Sunshine et al. 2007).

The forsterite mole percentages of asteroid (246) Asporina have been estimated to be between Fo60 and Fo90 by comparing the spectral curves of the olivine solid solution ranging from fayalite to forsterite (Cruikshank & Hartmann 1984). Sunshine & Pieters (1998) also estimated the composition of olivine on

<sup>4</sup> <http://smass.mit.edu/home.html>

**Table 6** Parameters Characterizing the VNIR Spectral Curves of Olivine before and after Irradiation

Olivine Samples	Reflectance (or albedo)			Reddening ( $R_{1800}/R_{700}$ )	SSDF
	700 nm	1050 nm	1800 nm		
OLV-original	0.7466	0.6052	0.8049	1.0781	0.7081
25 mJ*1 time	0.6626	0.5825	0.7772	1.1730	0.4114
25 mJ*2 times	0.6373	0.5856	0.7914	1.2418	0.2512
25 mJ*3 times	0.4810	0.4844	0.6972	1.4495	-0.0160
25 mJ*4 times	0.3612	0.3988	0.5727	1.5855	-0.2162
25 mJ*5 times	0.2752	0.3254	0.4716	1.7137	-0.3434

Eq. (6) expresses the calculation method of SSDF as an abbreviation for the stability of the spectral diagnostic features. When space weathering causes the olivine spectral slope to increase, the higher the SSDF value is, the clearer diagnostic features of the spectra become and the lower is degree of space weathering.

**Table 7** Final MGM Fitting Parameters of the Original Fresh and Irradiated Olivine Spectra with Method P

Olivine Samples	Center	Band M1–1		Center	Band M2		Center	Band M1–2		Estimated Fo#
		FWHM	Strength		FWHM	Strength		FWHM	Strength	
Original	844.6	173.5	-0.078	1025.9	176.2	-0.139	1197.9	421.3	-0.172	85.9
25mJ*1time	855.7	152.6	-0.046	1031.3	168.8	-0.121	1207.6	378.8	-0.129	76.2
25mJ*2times	862.9	158.0	-0.038	1033.9	162.4	-0.107	1203.8	376.3	-0.116	73.2
25mJ*3times	867.6	144.2	-0.025	1036.8	162.7	-0.098	1215.6	344.8	-0.092	66.6
25mJ*4times	869.3	145.1	-0.016	1040.3	161.2	-0.076	1223.8	314.1	-0.061	61.6
25mJ*5times	867.6	159.7	-0.012	1040.4	158.6	-0.054	1220.5	299.5	-0.039	63.1

The estimated Fo# result is the average of the predicted values of the three diagnostic bands.

**Table 8** Final MGM Fitting Parameters of the Original Fresh and Irradiated Olivine Spectra with Method E

Olivine Samples	Center	Band M1–1		Center	Band M2		Center	Band M1–2		Estimated Fo#
		FWHM	Strength		FWHM	Strength		FWHM	Strength	
Original	847.7	186.7	-0.086	1027.9	175.2	-0.145	1201.6	405.7	-0.170	83.1
25mJ*1time	855.1	170.9	-0.056	1032.0	165.9	-0.120	1200.3	394.5	-0.142	78.8
25mJ*2times	861.2	181.9	-0.050	1034.8	160.2	-0.107	1195.5	396.9	-0.131	76.6
25mJ*3times	864.7	188.9	-0.043	1037.3	159.5	-0.098	1200.6	382.7	-0.115	72.6
25mJ*4times	854.0	193.9	-0.038	1037.1	174.3	-0.089	1218.4	346.0	-0.089	70.9
25mJ*5times	844.3	296.3	-0.037	1039.9	184.5	-0.065	1222.5	333.8	-0.059	71.1

The estimated Fo# result is the average of the predicted values of the three diagnostic bands.

asteroids (246) Asporina using the MGM with some restrictions and concluded that it was likely greater than Fo80. For (354) Eleonora, Gaffey et al. (2015) reported that the Fo# estimate is from  $\sim$ Fo61 to  $\sim$ Fo71, while Sunshine et al. (2007) modified the temperature and quantified its Fo# to be  $\sim$ Fo90.

This paper smoothed the asteroids spectra and normalized at the maximum value to acclimatize to the MGM. Then, MGM was applied to deconvolve the spectra with an appropriate second-order polynomial continuum, as shown in Figure 15. The three diagnostic band centers of asteroid (246) Asporina spectrum are 860.97 nm, 1034.70 nm and 1235.21 nm, respectively. The predicted Mg-numbers are Fo63.0, Fo66.8 and Fo64.5, respectively, and the average number is  $\sim$ Fo65. Whereas, the three diagnostic band centers of asteroid (354) Eleonora spectrum are 847.85 nm, 1030.57 nm and 1214.13 nm, respectively, and the predicted Mg-numbers are Fo76.2, Fo74.4 and Fo81.9, respectively. The average number is  $\sim$ Fo78.

Based on the previous statement, space weathering may change the shape of spectral curves, and result in un-

derestimation of forsterite content. Based on Equation (6), the  $SSDF_{\text{olivine}}$  of asteroid (246) Asporina and (354) Eleonora are 0.3130 and 0.3105, respectively. Compared to the shape and  $SSDF_{\text{olivine}}$  of the irradiated olivine spectra featured in Figure 11 and Table 7, the spectral curves of the two asteroids are similar to the spectra of olivine irradiated with 25 mJ\*1 time and 25 mJ\*2 times. Moreover, the  $SSDF_{\text{olivine}}$  values of the two asteroids are also in between the  $SSDF_{\text{olivine}}$  values of these two irradiated olivine samples (0.4114  $\sim$  0.2512). This means there may be about 10 mol% forsterite underestimated. Therefore, considering the effects of space weathering on mineral chemical composition and the MGM deconvolution results, the Mg-numbers of asteroid (246) Asporina and (354) Eleonora are likely close to or greater than Fo75 and Fo88, respectively.

#### 4 CONCLUSIONS

MGM is a powerful tool to reveal the composition of mafic mineral assemblages. However, different continuum removal methods will affect the deconvolution result-

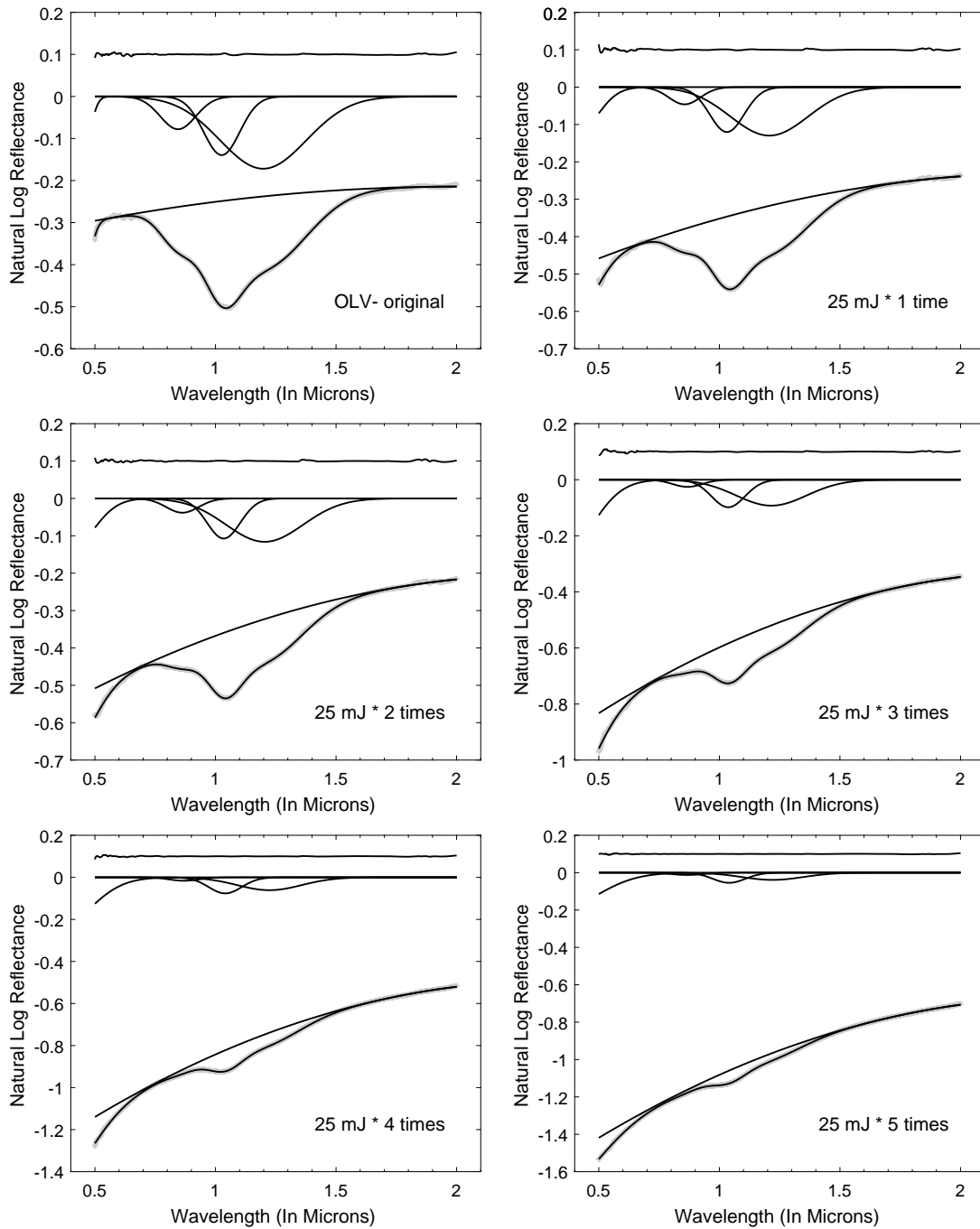


**Fig. 12** MGM fit to the spectra of original fresh and varying-degree irradiated olivine samples with Method P.

s. This paper explored the continuum removal method for the MGM on olivine diagnostic spectral features. It implemented four different types of continuum removal methods to get the olivine diagnostic spectral features, which have resulted in four different regression equation systems. In comparison with different regression equations obtained in this article and [Sunshine & Pieters \(1998\)](#), it is significant to highlight the following:

1) Flat line continuum removal method is the original choice by [Sunshine & Pieters \(1998\)](#), but it has many limi-

tations in the deconvolution of olivine spectra. This method can overestimate the visible region if the flat continuum is far from the *UV* band wings, which makes it not suitable for revealing spectra with slopes;

2) The oblique line continuum removal method is simple and feasible. The tangent continua contact the two inflection regions of the diagnostic feature. This method is suitable for an individual absorption region, but not for the whole band;

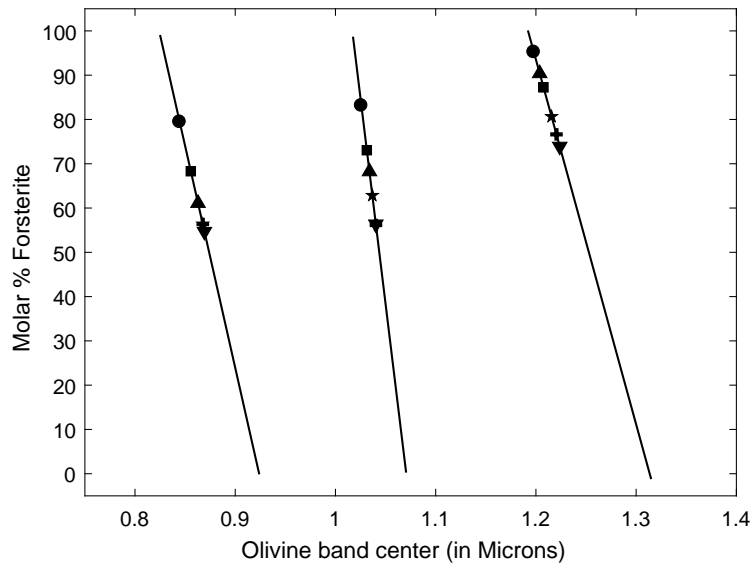


**Fig. 13** MGM fit to the original fresh and irradiated olivine spectra with Method P and prediction of the mole fraction of Fo#. Black circles correspond to original olivine sample. With increasing amount of radiation, the corresponding symbols are square, upward-pointing triangle, star, downward-pointing triangle and black cross respectively.

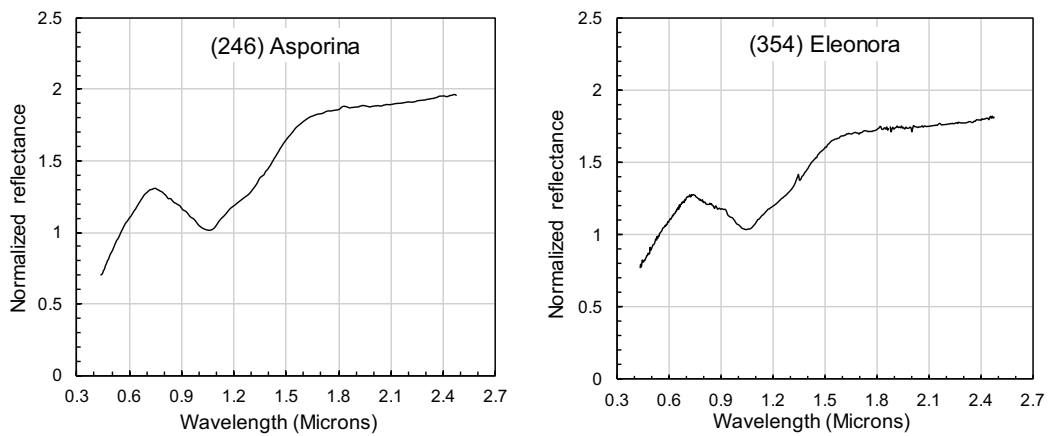


**Fig. 14** VNIR spectra of asteroids (246) Asporina and (354) Eleonora. The spectra are normalized to unity at 0.55  $\mu\text{m}$ .

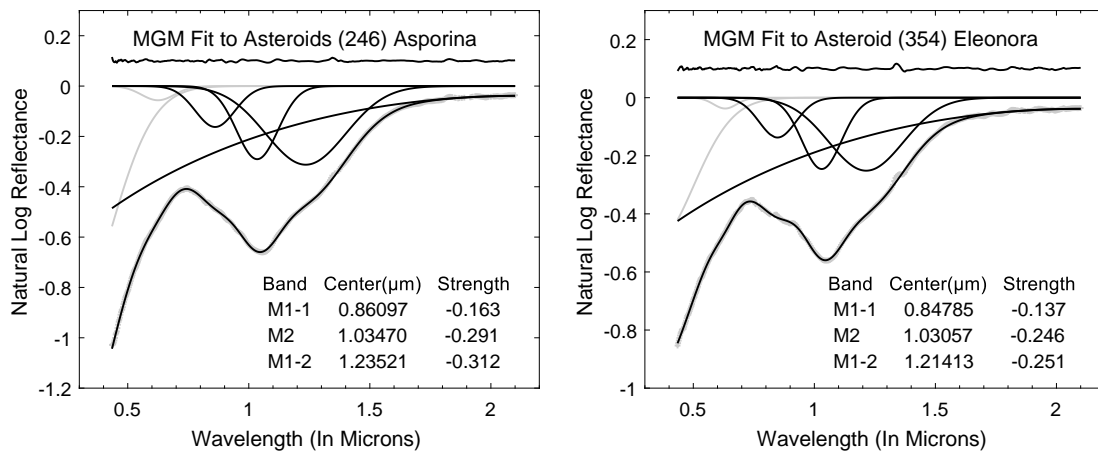


**Fig. 15** MGM deconvolution results of A-type asteroids (246) Asporina and (354) Eleonora.

3) A suitable second-order polynomial continuum removal method is also widely utilized, which is obviously superior to others. With this method, the overall shape of the continuum can describe the general spectral trend well;

4) An energy-wavelength polynomial continuum removal method is developed for deconvolving the reflectance spectra of lunar soils. This method does not perform well in laboratory spectra and the complex parameters are not friendly to the MGM program.

When applying a suitable second-order polynomial continuum removal method, we get the optimized Mg-number regression equations as displayed in Figure 8 and Table 2. The validation and analysis of the deconvolution results of olivine-dominated brachinite spectra indicate that the optimized Mg-number regression equations perform well for predicting the olivine composition in the laboratory. Furthermore, the effects of space weathering on the diagnostic spectral features of olivine are studied. The spectra of olivine irradiated with a pulse laser for simulating varying degrees of space weathering were analyzed with the MGM. The  $SSDF_{\text{olivine}}$  function was developed to quantify the stability of the spectral diagnostic features of olivine and its degree of space weathering, and this function is independent of absolute reflectance. The deconvolution results of the irradiated olivine spectra and their  $SSDF_{\text{olivine}}$  values verify that the estimation for forsterite proportion on the surface of A-type asteroids based on the telescopic spectra may be less than its actual chemical composition. However, the underestimated amount is still difficult to be accurately determined. In conclusion, there is a need for more research on space weathering to improve the applicability and accuracy of the MGM.

**Acknowledgements** This work was supported by the Foundation of the State Key Laboratory of Lunar and Planetary Sciences, Macau University of Science and Technology, Macau, China. The corresponding author X. Lu was also funded by The Science and Technology Development Fund, Macau SAR (No. 0018/2018/A). Y. Yang was supported by Beijing Municipal Science and Technology Commission (No. Z181100002918003). H. Zhang was supported by Natural Science Foundation of China (Nos. U1631124, 11773023 and 11941001). This work was also supported by grants from The Science and Technology Development Fund, Macau SAR (No. 0007/2019/A). We are very grateful to Hu Xiaoyi, Ma Pei and Jiang Te for their assistance in the experiments, whose comments and suggestions also improved the manuscript. Part of the spectral data utilized in this research were obtained and made available by the NASA RELAB Spectral Database at Brown University, Planetary Spectroscopy data at MIT and USGS Spectral Library. The MGM program was developed and provided by Brown University.

We acknowledge the support of Brown University, MIT and USGS. We also thank the anonymous reviewers and editors for their assistance in evaluating this paper.

## References

- Adams, J. B. 1974, *J. Geophys. Res.*, 79, 4829
- Antonenko, I., & Cloutis, E. A. 2003, Lunar and Planetary Science Conference, 34, 2095, eds. Mackwell, S., & Stansbery, Eileen
- Basilevsky, A. T., Shalygin, E. V., Titov, D. V., et al. 2012, *Icarus*, 217, 434
- Binzel, R. P., Rivkin, A. S., Thomas, C. A., et al. 2009, *Icarus*, 200, 480
- Bishop, J. L., Pieters, C. M., Hiroi, T., & Mustard, J. F. 1998, *Meteoritics & Planetary Science*, 33, 699
- Brunetto, R., Romano, F., Blanco, A., et al. 2006, *Icarus*, 180, 546
- Burbine, T. H., McCOY, T. J., Nittler, L. R., et al. 2002, *Meteoritics & Planetary Science*, 37, 1233
- Burns, R. G. 1970, *American Mineralogist*, 55, 1608
- Burns, R. G. 1974, *American Mineralogist*, 59, 625
- Chapman, C. R. 1996, *Meteoritics & Planetary Science*, 31, 699
- Chapman, C. R. 2004, *Annu. Rev. Earth Planet. Sci.*, 32, 539
- Clark, B. E., Hapke, B., Pieters, C., & Britt, D. 2002, *Asteroids III*, W. F. Bottke Jr., A. Cellino, P. Paolicchi, & R. P. Binzel (eds.) (Tucson: University of Arizona Press), 585
- Clark, R. N., & Roush, T. L. 1984, *Journal of Geophysical Research*, 89, 6329
- Clark, R. N., Swayze, G. A., Livo, K. E., et al. 2003, *Journal of Geophysical Research*, 108, 5131
- Clénet, H., Pinet, P., Daydou, Y., et al. 2011, *Icarus*, 213, 404
- Cloutis, E. A., & Bell III, J. F. 2000, *J. Geophys. Res: Planets*, 105, 7053
- Cruikshank, D. P., & Hartmann, W. K. 1984, *Science*, 223, 281
- De Leon, J., Duffard, R., Licandro, J., & Lazzaro, D. 2004, *A&A*, 422, L59
- Dyar, M., Sklute, E., Menzies, O., et al. 2009, *American Mineralogist*, 94, 883
- Fu, X., Zou, Y., Zheng, Y., & Ouyang, Z. 2012, *Icarus*, 219, 630
- Gaffey, M. J. 2010, *Icarus*, 209, 564
- Gaffey, M. J., Reddy, V., Fieber-Beyer, S., & Cloutis, E. 2015, *Icarus*, 250, 623
- Gallie, E., Lyder, D., Rivard, B., & Cloutis, E. 2008, *International Journal of Remote Sensing*, 29, 4089
- Green, R., Pieters, C., Mouroullis, P., et al. 2011, *Journal of Geophysical Research*, 116, E00G19
- Hapke, B. 2001, *J. Geophys. Res: Planets*, 106, 10039
- Hiroi, T., Pieters, C., & Noble, S. 2000, in 31st Annual Lunar and Planetary Science Conference, 31, 1548
- Hunt, G. R. 1977, *Geophysics*, 42, 501
- Hunt, G. R., & Ashley, R. P. 1979, *Econ. Geol.*, 74, 1613
- Isaacson, P. J., Pieters, C. M., Besse, S., et al. 2011, *Journal of Geophysical Research*, 116, E00G11

- Jin, S., Arivazhagan, S., & Araki, H. 2013, *Advances in Space Research*, 52, 285
- Kohout, T., Čuda, J., Filip, J., et al. 2014, *Icarus*, 237, 75
- Kokaly, R., Clark, R., Swayze, G., et al. 2017, USGS Spectral Library Version 7 Data., <https://pubs.er.usgs.gov/publication/ds1035>
- Li, C., Liu, D., Liu, B., et al. 2019, *Nature*, 569, 378
- Lindsay, S. S., Marchis, F., Emery, J. P., Enriquez, J. E., & Assafin, M. 2015, *Icarus*, 247, 53
- Lucey, P. G. 2004, *Geophys. Res. Lett.*, 31, L08701
- Lucey, P. G., Taylor, G. J., Hawke, B. R., & Spudis, P. D. 1998, *J. Geophys. Res: Planets*, 103, 3701
- Mittlefehldt, D. W., Bogard, D. D., Berkley, J. L., & Garrison, D. H. 2003, *Meteoritics & Planetary Science*, 38, 1601
- Miyazaki, T., Sueyoshi, K., & Hiraga, T. 2013, *Nature*, 502, 321
- Mustard, J. F., Poulet, F., Gendrin, A., et al. 2005, *Science*, 307, 1594
- Nehru, C., Prinz, M., Delaney, J., et al. 1983, *J. Geophys. Res: Solid Earth*, 88, B237
- Nehru, C., Prinz, M., Weisberg, M., et al. 1992, *Meteoritics*, 27, 267
- Nesvorný, D., Vokrouhlický, D., Morbidelli, A., & Bottke, W. F. 2009, *Icarus*, 200, 698
- Noble, S. K., Pieters, C. M., Hiroi, T., & Taylor, L. A. 2006, *J. Geophys. Res: Planets*, 111, E11009
- Ody, A., Poulet, F., Bibring, J. P., et al. 2013, *J. Geophys. Res: Planets*, 118, 234
- Ohtake, M., Matsunaga, T., Haruyama, J., et al. 2009, *Nature*, 461, 236
- Pieters, C. M., Fischer, E. M., Rode, O., & Basu, A. 1993, *J. Geophys. Res: Planets*, 98, 20817
- Pieters, C. M., & Mustard, J. F. 1988, *Remote Sensing of Environment*, 24, 151
- Pieters, C. M., Taylor, L. A., Noble, S. K., Keller, L. P., & Wentworth, S. 2000, *Meteoritics & Planetary Science Supplement*, 35, A127
- Pieters, C. M., Boardman, J., Buratti, B., et al. 2009, *Current Science*, 96, 500
- Pinet, P. C., Clenet, H., Heuripeau, F., et al. 2009, in *40th Lunar and Planetary Science Conference*, 40, 1612
- Rodger, A., Laukamp, C., Haest, M., & Cudahy, T. 2012, *Remote Sensing of Environment*, 118, 273
- Roush, T. L., Bishop, J. L., Brown, A. J., Blake, D. F., & Bristow, T. F. 2015, *Icarus*, 258, 454
- Salisbury, J. W., & Eastes, J. W. 1985, *Icarus*, 64, 586
- Salisbury, J. W., & Wald, A. 1992, *Icarus*, 96, 121
- Savitzky, A., & Golay, M. J. E. 1964, *Analytical Chemistry*, 36, 1627
- Shearer, C. K., & Papike, J. J. 1999, *American Mineralogist*, 84, 1469
- Singer, R. B. 1981, *Journal of Geophysical Research*, 86, 7967
- Staid, M. I., Pieters, C. M., Besse, S., et al. 2011, *Journal of Geophysical Research*, 116, E00G10
- Sugita, S., Nagata, K., Tsuboi, N., Hiroi, T., & Okada, M. 2011, in *42nd Lunar and Planetary Science Conference*, 42, 2624
- Sunshine, J. M., Bus, S. J., Corrigan, C. M., Mccoy, T. J., & Burbine, T. H. 2007, *Meteoritics & Planetary Science*, 42, 155
- Sunshine, J. M., Bus, S. J., Mccoy, T. J., et al. 2004, *Meteoritics & Planetary Science*, 39, 1343
- Sunshine, J. M., & Pieters, C. M. 1993, *J. Geophys. Res: Planets*, 98, 9075
- Sunshine, J. M., & Pieters, C. M. 1998, *J. Geophys. Res: Planets*, 103, 13675
- Sunshine, J. M., Pieters, C. M., & Pratt, S. F. 1990, *Journal of Geophysical Research*, 95, 6955
- Tarantola, A., & Valette, B. 1982, *Reviews of Geophysics*, 20, 219
- Taylor, S. R. 1978, *LPSC*, 9, 15
- Tonks, W. B., & Melosh, H. J. 1992, *J. Geophys. Res: Planets*, 98, 5319
- Tsuboi, N., Sugita, S., Hiroi, T., Nagata, K., & Okada, M. 2010, in *41st Lunar and Planetary Science Conference*, 41, 1744
- Wang, H., Ma, Y., Zhao, H., & Lu, X. 2017, *ChA&A*, 41, 419
- Wilson, L., & Head, J. W. 2017, *Journal of Volcanology and Geothermal Research*, 335, 113
- Wu, Y., Zhang, X., Yan, B., et al. 2010, *Science China (Physics, Mechanics & Astronomy)*, 53, 2160
- Yamamoto, S., Nakamura, R., Matsunaga, T., et al. 2010, *Nature Geoscience*, 3, 533
- Yang, Y., Zhang, H., Wang, Z., et al. 2017, *A&A*, 597, A50
- Zhang, H., Yang, Y., Jin, W., Liu, C., & Hsu, W. 2014, *Optics express*, 22, 21280
- Zhang, X., Ouyang, Z., Zhang, X., et al. 2016, *RAA (Research in Astronomy and Astrophysics)*, 16, 133